

Article

Transform-Limited Sub-100-fs Cr:ZnS Laser with a Graphene-ZnSe Saturable Absorber

Won Bae Cho * and Dong Ho Shin

Digital Biomedical Research Division, Electronics and Telecommunications Research Institute, Daejeon 34129, Republic of Korea; dhshin@etri.re.kr

* Correspondence: wbcho@etri.re.kr

Abstract: In this work, we present ultrashort pulse generation from passively mode-locked Cr:ZnS laser with a monolayer graphene-coated ZnSe substrate exhibiting high nonlinearity. The femtosecond Cr:ZnS laser produces output power up to 330 mW at a 233 MHz repetition rate. Even in the presence of an uneven negative dispersion profile, the enhanced self-phase modulation by the ZnSe substrate of the graphene saturable absorber enables the polycrystalline Cr:ZnS laser to produce slightly chirped 99 fs pulses at 2373 nm. With extracavity dispersion compensation using a mixture of 3 mm and 2 mm thick ZnSe plates, the pulse width was compressed from 99 fs to 73 fs, resulting in an improved time–bandwidth product from 0.431 to 0.318. Assuming a sech² pulse shape (0.315), the pulses were almost transform-limited. These results indicate that utilizing a graphene saturable absorber on a substrate with high nonlinearity presents an effective method for developing sub-100 fs solid-state lasers within the mid-IR spectral range.

Keywords: graphene-ZnSe; saturable absorber; mid-infrared laser; Cr:ZnS; passive mode-locking

1. Introduction

In recent years, there has been an increased demand for laser sources operating within the mid-infrared (mid-IR) range, covering from 2 to 5 μm . These laser sources are highly valuable in wide application fields, such as molecular spectroscopy, the generation of mid-IR supercontinuum, medical diagnostics, materials processing, and free-space communications [1–3]. The mid-IR spectral region, often referred to as the “molecular fingerprint” region, occupies a significant position in molecular spectroscopy due to its distinctive vibrational absorption characteristics across various molecules. Therefore, the demand for ultrafast and coherent mid-IR sources encompassing a wide spectral range remains a critical necessity, particularly for the progression of molecular spectroscopy. Mid-IR bulk lasers based on Cr²⁺-doped ZnS and ZnSe, characterized by broad emission cross-sections spanning 2.0 to 3.5 μm and often called the “Ti:sapphire of the mid-IR,” encompass a crucial section of the fingerprint region [1,3]. Thus, Cr²⁺:ZnSe (Cr:ZnSe) and the Cr²⁺:ZnS (Cr:ZnS) crystal with wide emission bands make it an attractive choice for developing ultrashort mid-IR solid-state lasers. Compared to Cr:ZnSe, the Cr:ZnS crystal distinguishes itself by exhibiting enhanced chemical and mechanical stabilities, a reduced thermal lensing parameter dn/dT , superior thermal conductivity, and a higher damage threshold [3]. These various features of the Cr:ZnS crystal establish it as a recommendable choice for the development of a high-power femtosecond mid-IR solid-state laser.

In recent years, Kerr-lens mode-locked Cr:ZnS laser has successfully generated < 29 fs pulses [4]. This approach, however, demands careful optical alignment and precise intracavity dispersion control for achieving ultrashort pulses. Furthermore, the mode-locked operation using polycrystalline gain media presents difficulties due to non-uniform grain distribution, leading to cavity misalignment power ramp-up [5].

Citation: Cho, W.B.; Shin, D.H. Transform-Limited Sub-100-fs Cr:ZnS Laser with a Graphene-ZnSe Saturable Absorber. *Photonics* **2023**, *10*, 1108. <https://doi.org/10.3390/photonics10101108>

Received: 1 September 2023

Revised: 22 September 2023

Accepted: 28 September 2023

Published: 30 September 2023



Copyright: © 2023 by the authors. Licensee MDPI, Basel, Switzerland. This article is an open access article distributed under the terms and conditions of the Creative Commons Attribution (CC BY) license (<https://creativecommons.org/licenses/by/4.0/>).

Consequently, significant endeavors are essential to establish stable Kerr-lens mode-locked mid-IR bulk lasers [1].

As a different strategy, ultrafast Cr²⁺-doped solid-state lasers have been demonstrated using passive mode-locking techniques, incorporating passive optical components such as semiconductor saturable absorber mirrors (SESAMs) [6,7], single-walled carbon nanotube saturable absorbers (SWCNT-SAs) [8,9], and graphene saturable absorbers (graphene-SAs) [10–12]. However, developing SESAMs and SWCNT-SAs for mid-IR bulk lasers involves obvious technical hurdles. These include the demand for complex epitaxial growth methods and the limited accessibility of commercial SWCNT materials with a sufficiently wide diameter enough to enable nonlinear absorption around 2.3 μm.

However, passive optical devices based on graphene, which are applicable to various photonics and optoelectronics devices [13–17], offer a range of benefits, such as exceptionally wide bandwidth, an economically efficient production process, and consistent saturable absorption properties when graphene is used as a saturable absorber [10,11]. Until now, several femtosecond Cr²⁺-doped bulk lasers with graphene saturable absorbers (graphene-SAs) have been demonstrated successfully [2,3]. To date, an ultrafast Cr:ZnS laser with graphene-SA generated ultrashort pulses with a duration of 41 fs [10], and continuous tuning across a broad wavelength spectrum (~300 nm) in the mode-locked operation was also demonstrated [11].

As shown in Table III in Ref. [2], a few mid-IR Cr²⁺-doped solid-state lasers with saturable absorbers were successful in achieving ultrashort pulses of <100 fs duration. However, to achieve < 100 fs pulses, the amount of intracavity group delay dispersion (GDD) should be precisely controlled [4,10]. Furthermore, it is essential to optimize intracavity dispersion to attain a uniform spectral profile across a broad range, a crucial factor in achieving ultrashort pulse durations. However, the fabrication of thick multilayer mirrors with uniform dispersion properties for mid-IR optical components poses a significant challenge [3]. Table 1 summarize the results of passively mode-locked sub-100 femtosecond Cr:ZnS solid-state lasers, which were updated based on Table III in Ref. [2]. The most successful results for achieving sub-100 fs pulses from Cr:ZnS lasers utilize Kerr-lens mode-locking techniques. However, only a few groups successfully generated ultrashort pulses using different passive mode-locking techniques, such as SESAMs, SWCNT, and graphene saturable absorbers. The results of this article are marked with bold style at the end of Table 1.

Table 1. Passively mode-locked < 100 femtosecond Cr:ZnS lasers operating near 2.4 μm spectral region. ML is the mode-locking, λ_{center} is the central wavelength, τ_p is the pulse duration, P_{out} is the maximum average output power, Frequency is the repetition rates, KLM is the Kerr-lens mode-locking, SESAM is the semiconducting saturable absorber mirror, CNTs is the single-walled carbon nanotubes, and Graphene is the monolayer graphene.

Laser crystal	ML technique	λ _{center} (nm)	τ _p (fs)	P _{out} (mW)	Frequency (MHz)	Reference
Cr ²⁺ :ZnS	KLM	2390	69	550	145	[18]
		2390	68	820	105	[19]
		2390	75	1000	210 ¹	[20]
		~2400	41	1900	79	[21]
		~2400	29	440	100	[4]
	SESAM	2370	79	800	250	[7]
	CNTs	2350	61	950	250	[8]
	Graphene	2400	49/41 ²	251/~75 ²	108/240 ²	[10]
		2373	73	330	233	This article

¹ Double-pulsing operation. ² Nitrogen purging and multi-pulsing operation.

In this study, we report the simple generation of ultrashort pulses (<100 fs) in the mid-IR spectral range using the enhanced self-phase modulation effect within the Cr:ZnS oscillator. For this purpose, we employed ZnSe as the base plate for developing transmission-type graphene saturable absorbers. ZnSe exhibits a higher nonlinear refractive index ($n_2 = 113 \pm 12 \times 10^{-20} \text{ m}^2/\text{W}$ at $2.3 \mu\text{m}$) compared to the ZnS ($n_2 = 47.8 \pm 5 \times 10^{-20} \text{ m}^2/\text{W}$), which is the host material for the Cr:ZnS laser crystal [22]. Furthermore, to increase intracavity power further, we decreased the output coupler's transmission from 15% to 5% in the cavity, as compared to a previously reported similar laser oscillator in Ref. [11]. Through the enhanced self-phase modulation effect in the oscillator, we successfully demonstrated a sub-100-fs Cr:ZnS laser with graphene-ZnSe saturable absorber, even in the presence of non-uniform round-trip dispersion spectra.

The femtosecond Cr:ZnS laser delivered an average output power of up to 330 mW at a repetition rate of 233 MHz. It produced slightly chirped 99 fs pulses with an 81.8 nm bandwidth centered at 2373 nm. With extracavity dispersion compensation using a combination of 3 mm and 2 mm thick ZnSe plates, the pulse width was compressed from 99 fs to 73 fs, improving the time–bandwidth product from 0.431 to 0.318. Assuming a sech² pulse shape (0.315), the pulses were almost transform-limited.

2. Passive Optical Switches Based on Graphene-ZnSe and Configuration of Cr:ZnS Laser

A similar fabrication technique detailed in reference [11] was applied for developing a high-quality graphene saturable absorber. Initially, we synthesized monolayer graphene through chemical vapor deposition on a copper (Cu) foil, followed by prompt cooling. Subsequently, we applied a supportive layer of 5 wt% polymethyl-methacrylate (PMMA) onto the graphene using a spin-coating technique. Following that, the copper layer underwent wet etching with ferric chloride (FeCl_3), which facilitated the transfer of both the graphene and PMMA layer onto 1 inch diameter zinc selenide (ZnSe) substrates. Finally, the PMMA layer was removed using acetone, resulting in the formation of a monolayer graphene saturable absorber on the ZnSe substrate, referred to as graphene-ZnSe SA.

Figure 1a depicts the linear optical characteristics of the graphene-ZnSe SA, and the insets show a photo of the developed graphene-ZnSe SA, with four dots on the ZnSe substrate, indicating the boundaries of the transferred monolayer graphene. The linear transmission curve reveals that the monolayer graphene deposited on a ZnSe substrate exhibits approximately 2% absorption near $2.3 \mu\text{m}$ [Appendix A], which is comparable to the theoretical value of $\pi\alpha = 2.3\%$. However, we have not yet characterized the nonlinear optical properties, such as the resonant response of the saturable absorption, the saturation fluence, and the modulation depth of the graphene-ZnSe SA near $2.3 \mu\text{m}$. Nevertheless, we expect a nonlinear response of the passive devices similar to ~ 2 ps reported in the reference [11], and comparable modulation depth of $\sim 0.4\%$ and saturation fluence of $\sim 14 \mu\text{J}/\text{cm}^2$ measured at near-IR wavelengths [23].

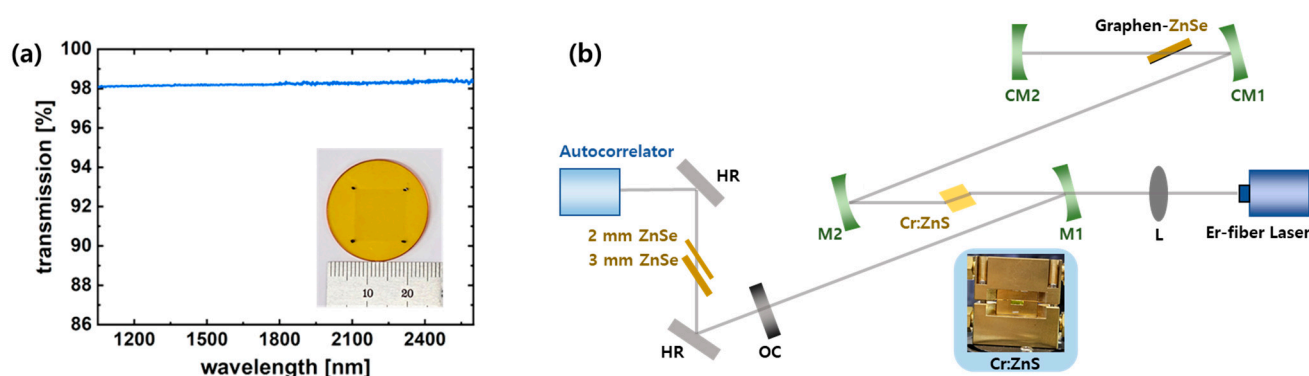


Figure 1. (a) Linear transmission and photographic images (inset) of graphene-ZnSe saturable absorber including a ruler. (b) Experimental setup of the passively mode-locked Cr:ZnS laser with graphene-ZnSe saturable absorber. Er-fiber Laser: linearly polarized continuous-wave Er-doped fiber laser, L: 100 mm pump focusing lens, M1 and M2: concave mirrors with ROC = -100 mm, CM1 and CM2: chirped mirrors with ROC = -75 mm, OC: output coupler with T = 5%, Graphene-ZnSe: monolayer graphene on the ZnSe substrate, 3 mm ZnSe: 3 mm thick ZnSe substrate, and 2 mm ZnSe: 2 mm thick ZnSe substrate. A photograph depicting Cr:ZnS laser crystal mounted on the copper block (inset).

For passive mode-locking of a polycrystalline Cr:ZnS laser employing graphene-ZnSe saturable absorbers, an astigmatically compensated Z-fold cavity configuration was used, as shown in Figure 1b. Linearly polarized 20 W Er-doped fiber laser (IPG Photonics) operating at 1550 nm was used as the pumping source. A rectangular, polycrystalline Cr:ZnS crystal, supplied by IPG Photonics, had a dimension of 6 mm (W) × 2 mm (H) × 5 mm (L). The 5 mm long Cr:ZnS crystal possesses a Cr²⁺ concentration of around $8.56 \times 10^{18} \text{ cm}^{-3}$, which yields a small signal absorption rate of about 94.2% at pump wavelength. After wrapping the crystal with indium foil to ensure efficient heat dissipation from the gain medium, the laser crystal was mounted in a water-cooled copper block whose temperature was stabilized at 15 °C, as shown in the inset of Figure 1b. The crystal was positioned at the Brewster angle to reduce reflection losses. The cavity waist for the gain medium was formed by two concave mirrors with a radius of curvature (ROC) of -100 mm, M1 and M2. As a focusing optic for the pump beam, a 100 mm plano-convex lens (L) was utilized. The waist size of the focused pump beam was calculated to be approximately 57 μm, while the waist size of the resonator beam varied between 65 μm and 75 μm depending on the distance between M1 and M2. These two beam sizes were similar, which enabled efficient energy transfer from the pump to the resonator beam. Two additional concave mirrors with ROC of -75 mm, CM1 and CM2, formed the second waist ($\omega_0 \approx 80\text{--}90 \text{ μm}$) in the longer cavity arm for the transmission-type graphene-ZnSe SA to obtain adequate energy fluence for bleaching the absorption of the passive devices. To minimize the insertion losses, the graphene-ZnSe SA was mounted at the Brewster angle near the focal point. At the other end of the resonator, a flat-wedged output coupler (OC) with 5% transmission at the lasing wavelength was installed. The distances between the optical components are as follows: M1 to the OC is approximately 188 mm, M1 to M2 is around 113 mm, M2 to M3 is 228 mm, and M3 to M4 is 114 mm. Consequently, the total round-trip distance covers roughly 643 mm. The design of the laser cavity is compact and occupies a footprint of 30 cm × 20 cm, except for the pump beam line. For extracavity dispersion compensation, 3 mm and 2 mm thick ZnSe plates were installed at the Brewster angle between the OC and the autocorrelator as shown in Figure 1b. To protect the oscillator from environmental variables like airflow and humidity, we encased Cr:ZnS laser only using acrylic blocks, but did not purge dry nitrogen gas to reduce humidity.

Figure 2a illustrates the wavelength-dependent group delay dispersion (GDD) of different optical components in the laser cavity: the high reflective mirror (M), chirped mirror (CM), output coupler (OC), a unit length (1 mm) of Cr:ZnS crystal, and ZnSe substrate. The theoretical GDD spectra of Cr:ZnS and ZnSe in Figure 2a were calculated using the Sellmeier equation for the individual materials, and the dispersion spectra for OC, M, and CM were provided by the producer (Layertec GmbH). Although concave mirrors of M1 and M2 in Figure 1b are characterized as “GDD reflection optimized” by Layertec, they were not specifically optimized for higher-order dispersion.

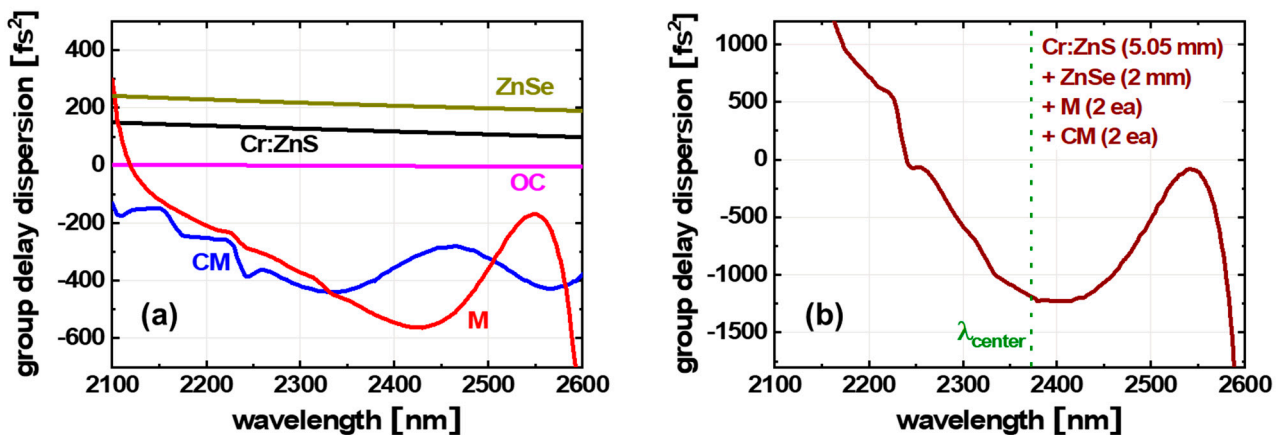


Figure 2. (a) Theoretical group delay dispersion (GDD) spectra of cavity components: 1 mm length Cr:ZnS (Cr:ZnS), 1 mm length ZnSe plate (ZnSe), output coupler (OC), GDD-optimized mirror (M), and chirped mirror (CM). (b) Net GDD spectra of the Cr:ZnS resonator with graphene-ZnSe saturable absorbers.

While the GDD of the 5% OC is almost close to 0 fs² in the lasing spectral ranges, the focusing concave mirrors (M1 and M2) exhibit negative dispersion between 2100 nm and 2600 nm. However, these mirrors were not designed to have ideally flat dispersion profiles within the spectral ranges; the “GDD-optimized” mirror (M) introduces an inhomogeneous and relatively strong negative GDD near 2430 nm as shown in Figure 2a. To mitigate the strong negative dispersion induced by M1 and M2 around 2430 nm, we employed a specially designed chirped mirror (CM) with a dispersion characteristic of $-300 (\pm 300)$ fs² between 2000 and 2700 nm, as depicted in Figure 2a. With two chirped mirrors (CM1 and CM2), the second focusing region was formed in the longer arm as shown in Figure 1b. This approach enabled to achieve flattened net-GDD profiles around 2400 nm, depicted in Figure 2b. In Figure 2b, the comprehensive round-trip GDD spectra are presented, incorporating parameters like the laser crystal’s thickness, the ZnSe substrate’s thickness for the SA, and the count of GDD-optimized mirrors and chirped mirrors. By employing four concave mirrors (M1, M2, CM1, and CM2), we effectively compensated for the positive dispersion introduced by the Cr:ZnS laser crystal and ZnSe substrate of the SA. As shown in Figure 2b, the calculated overall intracavity dispersion was approximately -1200 fs² at ~ 2370 nm, denoted by the dashed vertical green lines, indicating the center wavelength of the passively mode-locked Cr:ZnS laser using the graphene-ZnSe SA.

However, it is significant to note that the GDD values exhibited for the mirrors in Figure 2a are based on simulation data under normal incidence (0 degrees). Consequently, due to the folding angle of 15 degrees introduced by the three mirrors (M1, M2, and CM1), the practical cavity round-trip dispersion might change from the approximated values shown in Figure 2b. In this configuration, soliton mode-locking within the negative dispersion regime was achieved through slight vibrations applied to the output coupler [24].

3. Femtosecond Cr:ZnS Laser with a Graphene-ZnSe Saturable Absorber

Utilizing a graphene-ZnSe saturable absorber, we successfully demonstrated a passively mode-locked Cr:ZnS laser and studied its output characteristics, as depicted in Figure 3. Figure 3a presents the measured laser output powers, with the solid vertical black line indicating the mode-locking threshold achieved at an output power of 104 mW at incident pump power of 2.19 W. By employing 5% output couplers in the oscillator, we achieved output powers of up to 330 mW at 5.9 W pump power. The Cr:ZnS laser exhibited stable mode-locking across the entire power range above the mode-locking threshold and could be maintained for several hours. Additionally, no visible damage to the graphene-ZnSe saturable absorber was observed. While higher output power could be

achieved by increasing the pump power, this led to undesirable continuous wave (CW) components and multiple pulsing that disrupted the stable mode-locked operation. The spectrum broadening with increasing output power is shown in Figure 3b. Each output spectrum was measured using the WaveScan USB (A.P.E GmbH) with a wavelength resolution of ± 0.2 nm within the range of 1000 to 2600 nm.

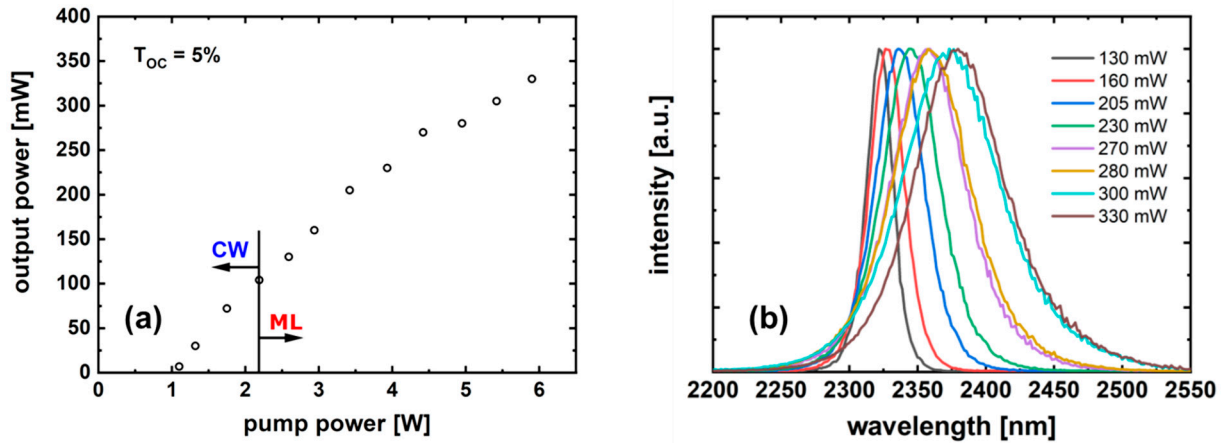


Figure 3. Graphene-ZnSe mode-locked Cr:ZnS laser: (a) measured output power (CW: continuous wave, ML: mode-locking), and the solid black line denotes the mode-locking threshold, and (b) output optical spectrum at different laser powers.

Figure 4 displays the laser spectrum and the intensity autocorrelation trace, both recorded at an output power of approximately 300 mW. The autocorrelation trace was obtained using the PulseCheck USB MIR from A.P.E GmbH. The spectral bandwidth (FWHM) of the pulses measured 81.8 nm at a central wavelength of 2373 nm. The slightly noisy spectrum observed above 2400 nm in Figure 4a is attributed to intracavity atmospheric absorption [3]. In Figure 4b, indicated by a black circle, the concurrently measured pulse width was 99 fs, leading to a time–bandwidth product of 0.431. This value indicates that the generated pulses were slightly chirped.

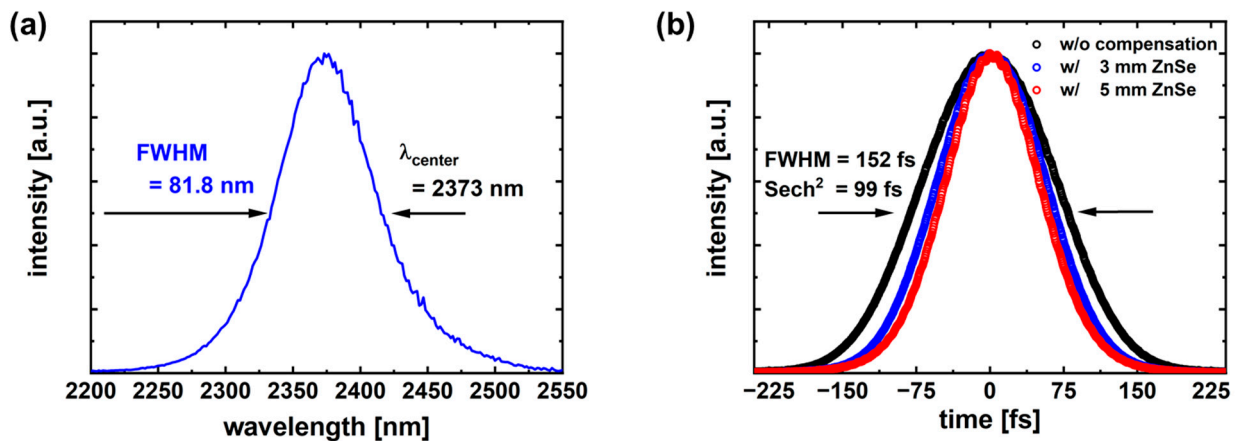


Figure 4. Femtosecond Cr:ZnS laser with graphene-ZnSe saturable absorber: (a) optical spectrum and (b) intensity autocorrelation trace without extracavity dispersion compensation (black circle) and with extracavity dispersion compensation using 3 mm thick (blue circle) and 5 mm thick (3 mm + 2 mm, red circle) ZnSe plates.

The intracavity positive dispersion of the Cr:ZnS laser was only compensated with mirrors possessing negative dispersion properties, leading to difficulties in controlling the intracavity dispersion accurately. To achieve Fourier transform-limited pulses, we introduced an extracavity dispersion compensator using ZnSe plates, which provided a positive GDD of 210 fs² per 1 mm thick ZnSe at 2370 nm. To minimize reflection losses, these plates were positioned at the Brewster angle between the output coupler and the autocorrelator. Additionally, high reflectance (HR) mirrors (~ 0 fs² @ 45 degrees) were employed to guide the beam toward the autocorrelator and minimize additional dispersion from external optical components.

As shown in Figure 4b, with the installation of a 3 mm thick ZnSe plate, the pulse width decreased from 99 fs to 81 fs, yielding a time–bandwidth product of 0.353, which was close to the transform-limited value for a sech² pulse (0.315). Adding an extra 2 mm thick ZnSe plate further reduced the pulse duration to 73 fs, resulting in a time–bandwidth product of 0.318. This value was almost identical to the theoretical value for a sech² pulse (0.315), as shown in Figure 5. Compared to other laser cavities with similar round-trip GDD values of around -1000 fs² and relatively flat dispersion profiles [1,7], the Cr:ZnS laser with graphene-ZnSe successfully generates <100 fs pulses through the enhanced self-phase modulation effect induced by the ZnSe substrate of the saturable absorber, even in the presence of inhomogeneous dispersion spectra. Therefore, an even shorter pulse width can be achieved by further optimizing the negative dispersion profile to be flat.

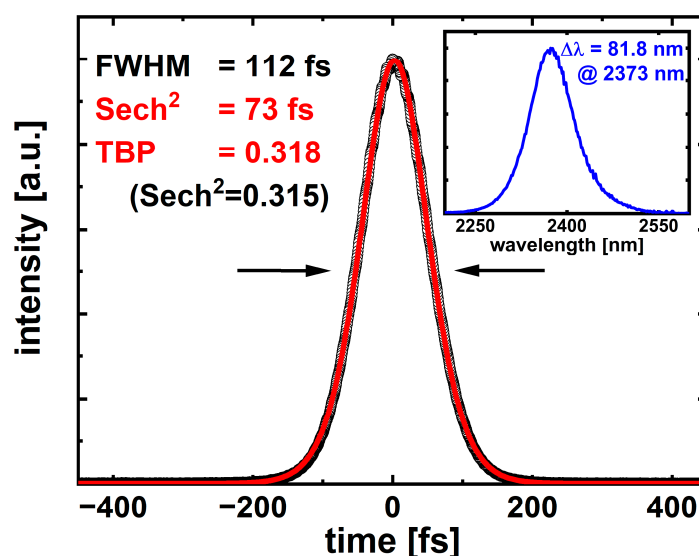


Figure 5. Extracavity dispersion compensated autocorrelation trace and the corresponding laser spectrum (inset) of the femtosecond Cr:ZnS laser with graphene-ZnSe saturable absorber.

The radio-frequency (RF) spectrum of the femtosecond Cr:ZnS laser was also measured in different spans to verify the stable mode-locked operation, as shown in Figure 6. The first beat note at 233.13 MHz displayed a pedestal peak separation of around 62 dB above carrier (dBc), recorded with a resolution bandwidth of 100 Hz within a 200 kHz span. This high signal-to-noise ratio of RF spectra and wider 1 GHz span measurement (Figure 6b) clearly indicates a stable and clean CW mode-locked operation without any undesired laser operation, such as Q-switching instability or multiple-pulsing.

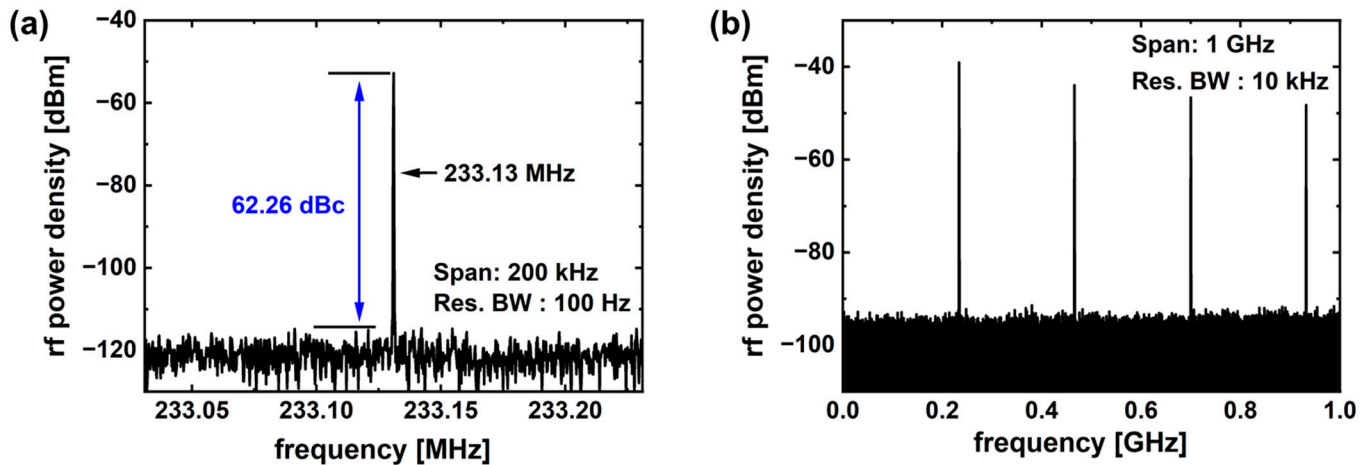


Figure 6. RF trace of the passively mode-locked Cr:ZnS laser with graphene-ZnSe: (a) the fundamental beat note at 233.13 MHz and (b) 1 GHz span of the RF spectrum.

4. Discussion

Transmission-type graphene SAs offer three distinct advantages over reflection-type SAs, despite the need for a second focusing regime in the oscillator to ensure adequate energy fluence for the saturable absorber (SA):

1. Transmitting graphene SAs typically consist of a graphene layer with widespread linear optical absorption properties and a transparent supporting substrate. This design allows the graphene SA to operate across an exceptionally wide spectral range.
2. Precise control of energy fluence on the graphene SA is achieved by simply adjusting its position within the focusing regime for laser performance optimization.
3. Changing the substrate material of the transmitting SA enables control over the amount of self-phase modulation effect within the resonator.

Especially noteworthy is the third advantage of the transmitting graphene SA, which assists in the relatively easy achievement of sub-100 fs pulses in the mid-IR spectral regime. As we explained in the Introduction section, achieving sub-100 fs pulses from polycrystalline Cr:ZnS lasers demands precise control of intracavity dispersion and the establishment of a uniform dispersion profile across a broad spectral range [4]. However, fabricating mid-IR mirrors with uniform dispersion is not a trivial task due to thick multilayer dielectric coatings [3]. Therefore, by simply exchanging the previous widely used SA's baseplate with low nonlinearity for a baseplate with high nonlinearity, it is possible to achieve shorter pulse durations through the enhanced nonlinear self-phase modulation effect.

Until now, CaF₂ substrates with low nonlinearity have been widely employed as the baseplate for fabricating transmitting graphene SAs in the mid-IR spectral regime [11,12]. CaF₂ possesses a small nonlinear refractive index ($n_2 = 1.09 \pm 0.11 \times 10^{-20} \text{ m}^2/\text{W}$), resulting in negligible nonlinear effects within the cavity. The nonlinearity of CaF₂ is approximately two orders of magnitude smaller than that of ZnSe [22]. However, ZnSe has higher refractive indices ($n = 2.43$) compared to CaF₂ ($n = 1.42$) at 2340 nm; ZnSe has a Brewster angle of 67.7°, while CaF₂ has a Brewster angle of 54.9°. Consequently, by increasing the effective focused beam spot size on the graphene-ZnSe SA with a high Brewster's angle, both the laser mode-locking threshold and the sensitivity of optical alignment would also be increased. However, the enhanced self-phase modulation effects induced by the ZnSe substrate of the graphene SA meaningfully facilitated the relatively easier attainment of ultrashort pulses in the mid-IR range.

5. Conclusions

In conclusion, we have successfully demonstrated a passively mode-locked polycrystalline Cr:ZnS laser utilizing a monolayer graphene-coated ZnSe substrate with high nonlinearity. The femtosecond Cr:ZnS laser delivered an average output power of up to 330 mW at a repetition rate of 233 MHz. Utilizing the enhanced self-phase modulation effects from the ZnSe plate of the saturable absorber, the femtosecond Cr:ZnS laser generated slightly chirped 99 fs pulses with a bandwidth of 81.8 nm at a center wavelength of 2373 nm, even under the conditions of inhomogeneous negative dispersion spectra. With extracavity dispersion compensation utilizing a total ZnSe plate length of 5 mm, the pulse width was dramatically compressed from 99 fs to 73 fs, resulting in an improved time–bandwidth product of 0.318 compared to the initial value of 0.431. Assuming a sech^2 pulse shape (0.315), the generated pulses were almost transform-limited. These results demonstrate that a graphene saturable absorber with a highly nonlinear substrate provides a simple approach for developing ultrashort femtosecond lasers in the mid-IR spectral regime.

Author Contributions: Conceptualization, W.B.C.; methodology, W.B.C.; software, W.B.C.; validation, W.B.C.; formal analysis, W.B.C.; investigation, W.B.C.; resources, W.B.C.; data curation, W.B.C.; writing—original draft preparation, W.B.C. and D.H.S.; writing—review and editing, W.B.C. and D.H.S.; visualization, W.B.C.; supervision, W.B.C. and D.H.S.; project administration, D.H.S.; funding acquisition, D.H.S. All authors have read and agreed to the published version of the manuscript.

Funding: This work was supported by Institute for Information & Communications Technology Planning & Evaluation (IITP) grant funded by the Korea government (MSIT) (No. RS-2023-00230545).

Institutional Review Board Statement: Not applicable.

Informed Consent Statement: Not applicable.

Data Availability Statement: Data sharing not applicable.

Conflicts of Interest: The authors declare no conflicts of interest.

Appendix A

The linear transmission spectra of a graphene-ZnSe saturable absorber, comprising a monolayer graphene transferred onto a ZnSe substrate with high nonlinearity.

We measured the linear transmission of graphene saturable absorbers using spectrophotometers (Lambda 1050, Perkin Elmer, USA). Two substrates, both 2 mm thick, were prepared for the measurements: one was a bare ZnSe substrate, and the other had a monolayer of graphene transferred onto a ZnSe substrate. Each sample was loaded into the spectrophotometers, and the transmission was recorded, as shown in Figure A1a. In Figure A1a, “ZnSe substrate” represents a bare 2 mm thick ZnSe plate, while “graphene-ZnSe” indicates a ZnSe plate with graphene deposited on it. The changes in transmission observed near the 1800 nm range were a result of the exchange of the optical source used in the spectrophotometer.

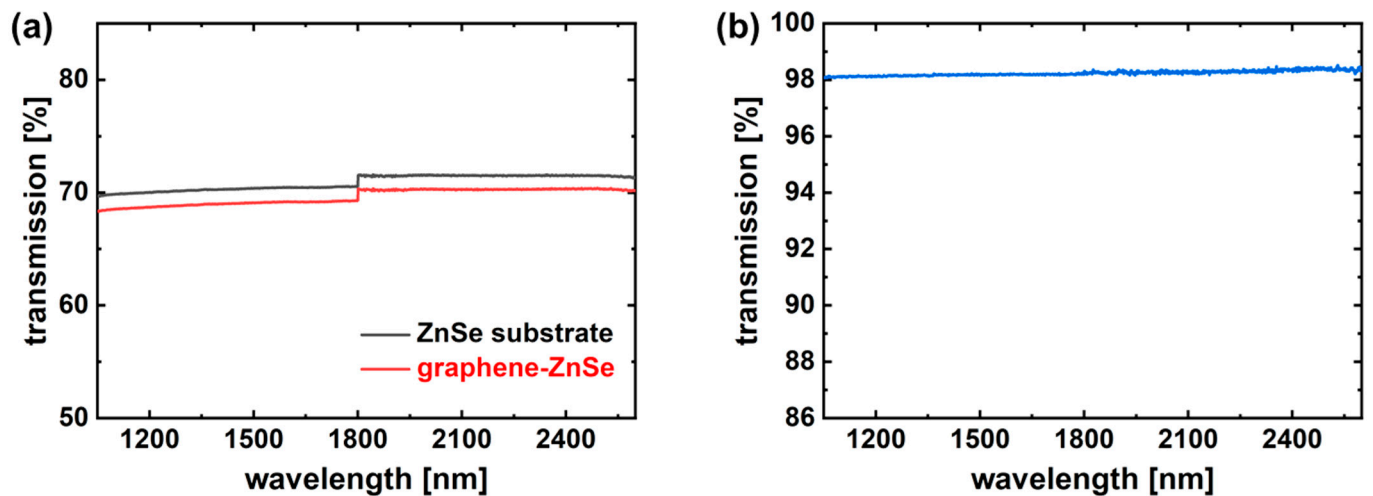


Figure A1. Linear transmission spectra of the graphene-ZnSe saturable absorber: (a) transmission curve of the bare substrate (ZnSe with 2 mm thickness) and the graphene saturable absorber (graphene-ZnSe) and (b) transmission spectra of the monolayer graphene, which was transferred on ZnSe substrate.

To achieve the transmittance spectrum of monolayer graphene only, $T_{\text{graphene-ZnSe}}$ was divided by $T_{\text{bare ZnSe}}$ as follows.

$$T_{\text{graphene}} = \frac{T_{\text{graphene-ZnSe}}}{T_{\text{bare ZnSe}}}$$

The linear transmission spectrum of the monolayer graphene saturable absorber demonstrates approximately 1.8% absorption at 2300 nm, a slight deviation from the theoretically expected universal absorption value of 2.3% [25].

References

1. Mirov, S.B.; Fedorov, V.V.; Martyshkin, D.; Moskalev, I.S.; Mirov, M.; Vasilyev, S. Progress in Mid-IR Lasers Based on Cr and Fe-Doped II–VI Chalcogenides. *IEEE J. Sel. Top. Quantum Electron.* **2015**, *21*, 292–310. <https://doi.org/10.1109/jstqe.2014.2346512>.
2. Ma, J.; Qin, Z.; Xie, G.; Qian, L.; Tang, D. Review of mid-infrared mode-locked laser sources in the 2.0 μm –3.5 μm spectral region. *Appl. Phys. Rev.* **2019**, *6*, 021317. <https://doi.org/10.1063/1.5037274>.
3. Sorokina, I.T.; Sorokin, E. Femtosecond Cr²⁺-Based Lasers. *IEEE J. Sel. Top. Quantum Electron.* **2015**, *21*, 273–291. <https://doi.org/10.1109/jstqe.2014.2341589>.
4. Vasilyev, S.; Moskalev, I.; Mirov, M.; Mirov, S.; Gapontsev, V. Three optical cycle mid-IR Kerr-lens mode-locked polycrystalline Cr²⁺:ZnS laser. *Opt. Lett.* **2015**, *40*, 5054–5057. <https://doi.org/10.1364/OL.40.005054>.
5. Baudrier-Raybaut, M.; Haidar, R.; Kupecek, P.; Lemasson, P.; Rosencher, E. Random quasi-phase-matching in bulk polycrystalline isotropic nonlinear materials. *Nature* **2004**, *432*, 374–376. <https://doi.org/10.1038/nature03027>.
6. Sorokin, E.; Tolstik, N.; Schaffers, K.I.; Sorokina, I.T. Femtosecond SESAM-modelocked Cr:ZnS laser. *Opt. Express* **2012**, *20*, 28947–28952. <https://doi.org/10.1364/OE.20.028947>.
7. Barh, A.; Heidrich, J.; Alaydin, B.O.; Gaulke, M.; Golling, M.; Phillips, C.R.; Keller, U. Watt-level and sub-100-fs self-starting mode-locked 2.4-mm Cr:ZnS oscillator enabled by GaSb-SESAMs. *Opt. Express* **2021**, *29*, 5934–5946. <https://doi.org/10.1364/OE.416894>.
8. Tolstik, N.; Okhotnikov, O.; Sorokin, E.; Sorokina, I.T. Femtosecond Cr:ZnS laser at 2.35 μm mode-locked by carbon nanotubes. *Proc. SPIE* **2014**, 8959, 89591A.
9. Okazaki, D.; Arai, H.; Anisimov, A.; Kauppinen, E.I.; Chiashi, S.; Maruyama, S.; Saito, N.; Ashihara, S. Self-starting mode-locked Cr:ZnS laser using single-walled carbon nanotubes with resonant absorption at 2.4 μm . *Opt. Lett.* **2019**, *44*, 1750–1753. <https://doi.org/10.1364/OL.44.001750>.
10. Tolstik, N.; Sorokin, E.; Sorokina, I.T. Graphene mode-locked Cr:ZnS laser with 41 fs pulse duration. *Opt. Express* **2014**, *22*, 5564–5571. <https://doi.org/10.1364/OE.22.005564>.
11. Cho, W.B.; Choi, S.Y.; Zhu, C.; Kim, M.H.; Kim, J.W.; Kim, J.S.; Park, H.J.; Shin, D.H.; Jung, M.Y.; Wang, F.; et al. Graphene mode-locked femtosecond Cr²⁺:ZnS laser with \sim 300 nm tuning range. *Opt. Express* **2016**, *24*, 20774–20780. <https://doi.org/10.1364/OE.24.020774>.

12. Cizmeciyan, M.N.; Kim, J.W.; Bae, S.; Hong, B.H.; Rotermund, F.; Sennaroglu, A. Graphene mode-locked femtosecond Cr:ZnSe laser at 2500 nm. *Opt. Lett.* **2013**, *38*, 341–343.
13. Bonaccorso, F.; Sun, Z.; Hasan, T.; Ferrari, A.C. Graphene photonics and optoelectronics. *Nat. Photonics* **2010**, *4*, 611–622. <https://doi.org/10.1038/nphoton.2010.186>.
14. Chen, Z.; Cai, P.; Wen, Q.; Chen, H.; Tang, Y.; Yi, Z.; Wei, K.; Li, G.; Tang, B.; Yi, Y. Graphene Multi-Frequency Broadband and Ultra-Broadband Terahertz Absorber Based on Surface Plasmon Resonance. *Electronics* **2023**, *12*, 2655. <https://doi.org/10.3390/electronics12122655>.
15. Lai, R.; Shi, P.; Yi, Z.; Li, H.; Yi, Y. Triple-Band Surface Plasmon Resonance Metamaterial Absorber Based on Open-Ended Prohibited Sign Type Monolayer Graphene. *Micromachines* **2023**, *14*, 953. <https://doi.org/10.3390/mi14050953>.
16. Tang, B.; Ren, Y. Tunable and switchable multi-functional terahertz metamaterials based on a hybrid vanadium dioxide-graphene integrated configuration. *Phys. Chem. Chem. Phys.* **2022**, *24*, 8408–8414. <https://doi.org/10.1039/d1cp05594a>.
17. Ye, Z.; Wu, P.; Wang, H.; Jiang, S.; Huang, M.; Lei, D.; Wu, F. Multimode tunable terahertz absorber based on a quarter graphene disk structure. *Results Phys.* **2023**, *48*, 106420. <https://doi.org/10.1016/j.rinp.2023.106420>.
18. Tolstik, N.; Sorokin, E.; Sorokina, I.T. Kerr-lens mode-locked Cr:ZnS laser. *Opt. Lett.* **2013**, *38*, 299–301. <https://doi.org/10.1364/OL.38.000299>.
19. Tolstik, N.; Sorokin, E.; Sorokina, I.T. Watt-level Kerr-Lens Mode-Locked Cr:ZnS Laser at 2.4 μm . In Proceedings of the CLEO: 2013, San Jose, CA, USA, 9 June 2013; p. CTh1H.2.
20. Sorokin, E.; Tolstik, N.; Sorokina, I. 1 Watt Femtosecond mid-IR Cr:ZnS Laser; *Proc. SPIE* **2013** 8599, 859916.
21. Vasilyev, S.; Mirov, M.; Gapontsev, V. Mid-IR Kerr-Lens Mode-Locked Polycrystalline Cr²⁺:ZnS Laser with 0.5 MW Peak Power. In Proceedings of the Advanced Solid State Lasers, Berlin, Germany, 4 October 2015; p. AW4A.3.
22. Patwardhan, G.N.; Ginsberg, J.S.; Chen, C.Y.; Jadidi, M.M.; Gaeta, A.L. Nonlinear refractive index of solids in mid-infrared. *Opt. Lett.* **2021**, *46*, 1824–1827. <https://doi.org/10.1364/OL.421469>.
23. Cho, W.B.; Kim, J.W.; Lee, H.W.; Bae, S.; Hong, B.H.; Choi, S.Y.; Baek, I.H.; Kim, K.; Yeom, D.-I.; Rotermund, F. High-quality, large-area monolayer graphene for efficient bulk laser mode-locking near 1.25 μm . *Opt. Lett.* **2011**, *36*, 4089–4091.
24. Kärtner, F.X.; Jung, I.D.; Keller, U. Soliton mode-locking with saturable absorbers. *IEEE J. Sel. Top. Quantum Electron.* **1996**, *22*, 540–556.
25. Nair, R.R.; Blake, P.; Grigorenko, A.N.; Novoselov, K.S.; Booth, T.J.; Stauber, T.; Peres, N.M.R.; Geim, A.K. Fine Structure Constant Defines Visual Transparency of Graphene. *Science* **2008**, *320*, 1308–1308. <https://doi.org/10.1126/science.1156965>.

Disclaimer/Publisher’s Note: The statements, opinions and data contained in all publications are solely those of the individual author(s) and contributor(s) and not of MDPI and/or the editor(s). MDPI and/or the editor(s) disclaim responsibility for any injury to people or property resulting from any ideas, methods, instructions or products referred to in the content.